AD-A134 197 AN APPROACH TO ROTATION INVARIANT TEXTURE CLASSIFICATION AND SOME EXPERIM..(U) PURDUE UNIV LAFAYETTE IN SCHOOL OF ELECTRICAL ENGINEERING 1/1

UNCLASSIFIED R L KASHYAP ET AL. AUG 83 TR-EE-83-26 F/G 12/1 NL

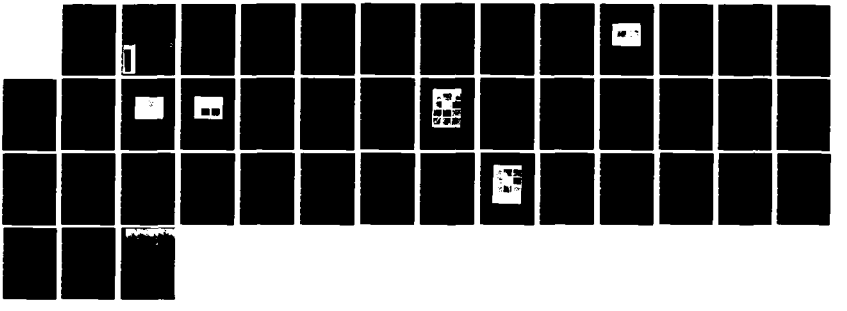

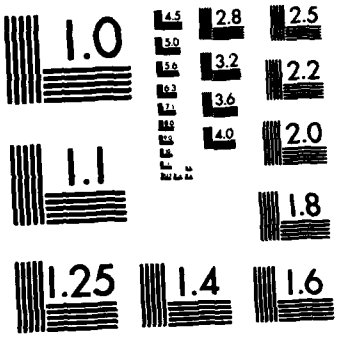

(12)

An Approach to Rotation Invariant Texture Classification & Some Experimental Results

R. L. Kashyap
A. Khotanzad

TR-EE 83-26
August 1983

School of Electrical Engineering
Purdue University
West Lafayette, Indiana 47907

A Technical Report

Under Grant No. N00014-82-K-0360

AN APPROACH TO ROTATION INVARIANT TEXTURE CLASSIFICATION AND SOME EXPERIMENTAL RESULTS

Submitted to :

Dr. Lloyd Griffiths

Electronics Division

Office of Naval Research

800 N. Quincy Street

Arlington, VA 22217

Submitted by :

R. L. Kashyap and A. Khotanzad

School of Electrical Engineering

ADVANCED AUTOMATION RESEARCH LABORATORY

PURDUE UNIVERSITY

WEST LAFAYETTE, INDIANA, 47907

Report no. TR-EE-83-26

August 1983

A-1

TABLE OF CONTENTS

Abstract:

This paper presents a new feature extraction method for classifying a texture image into one of the n possible classes, C_i, i=1,...,n. The extracted features are invariant under rotation or gray scale changes. Two types of random field models namely, Circular Auto Regressive model, and Simultaneous Auto Regressive model are used to extract these features. These models are fitted to a given M×M digitized image and their parameters are estimated. These estimated parameters and some functions of them constitute the desired rotation invariant feature vector. The classification power of this feature vector is demonstrated through experimental results obtained with twelve different classes of natural textures including both macrotextures and microtextures.

Research supported by the Office of Naval Research through Grant N00014-82-K-0360

1. Introduction

Analysis and classification of the texture of digitized images has been the focus of interest for the last 20 years. Briefly stated, there are a finite number of classes C_i, i=1,...,n. A number of so called training images belonging to each class are available. Based on the information extracted from these sets a rule is designed which classifies a given test image of unknown class to one of the n classes. The key step in any classification problem is the choice of a set of features which reduces the dimension of data to a computationally reasonable amount while preserving much of the classifying information present in the actual data.

A number of approaches to the texture analysis and classification problem have been developed over the years. Most of the popular statistical methods presented in the literature use features which are not rotation invariant. Moreover these features generally result in accuracy rates in the 80+ percent range which is not very impressive. More details about these methods and their classification power could be found in [14] and [17]. The aim of this paper is to develop an algorithm for extracting features from a texture and classifying it when the orientation of the test or training sample is arbitrary, i.e. the accuracy of classification is not affected by the rotation of the texture. To achieve this, a new model called circular auto regressive (CAR) random field model is developed whose parameters are rotation invariant. The CAR parameters along with two more features representing fineness and directionality in the texture make up our rotation invariant feature set. The other two features are obtained from simultaneous auto regressive (SAR) random field models discussed in [15]. Experimental results with different natural textures indicates that a strong classification power is associated with

our rotation invariant feature set.

2. Circular Auto Regressive (CAR) Random Field Model

Let $\{y(s), s=(s_1,s_2)\in\Omega\}$ be the set of intensity values of a given M×M digitized discrete image, $\Omega=\{(s_1,s_2),\ 0 \le s_1,s_2 \le M-1\}$. These intensities are only available on rectangular grids, meaning that s_1 and s_2 could only have integer values. The intensity value of any other point y(i,j) where (i,j) does not correspond to a grid corner, is not given and may be interpolated.

We assume that $\{y(s), s\in\Omega\}$ is a realization of an underlying circular auto regressive random field model,

$$y(s) = \alpha \sum_{r\in N_{1c}} y(s\oplus r) + \sqrt{\beta}\omega(s), \qquad s\in\Omega \tag{1}$$

$$r = (r_1,r_2).$$

A finite lattice toroidal structure is assumed for the image, therefore $\oplus$ implies addition modulo M. The circular neighbor set N_{1c} consists of 8 symmetrical pixels, all of which are located on a circle in the image plane centered at s with a radius of one. N_{1c} is illustrated in Fig. 1. $\omega(s)$ in (1) is a sequence of i.i.d. random numbers with zero mean and unit variance. α and β are the parameters of the model. Note that (1) represents a model for a purely circularly symmetric (isotropic) texture.

Four of the pixels of N_{1c} correspond to grid corners and therefore their intensity values are available. These four are pixels directly to the left, right, above and below the pixel under study. The other four diagonal and off-diagonal pixels do not fall on the grid points and their intensities should be interpolated. Let $t = (t_1,t_2)$ be one such pixel. Take $s^{(i)}$, i=1,2,3,4 as the

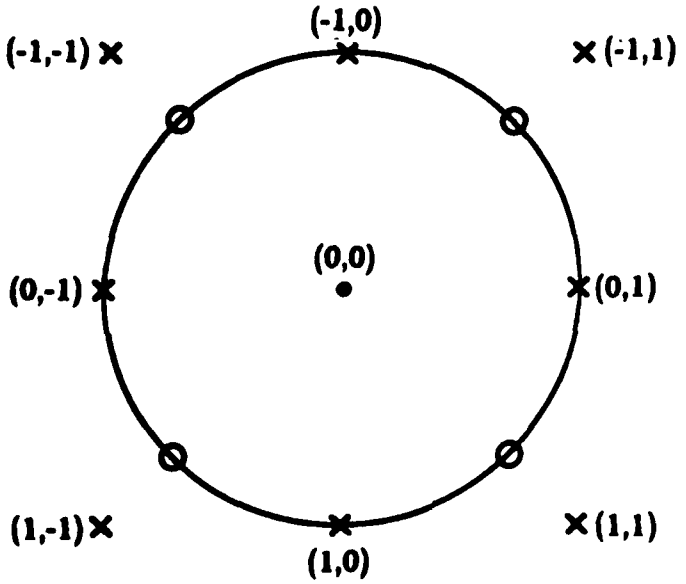

Figure 1: Circular neighbor set N_c
•, X = original grid points
0 = Interpolated pixels

coordinates of the four nearest grid points surrounding t. $\{y(s^{(i)}), i=1,2,3,4\}$ is an obvious candidate from which y(t) could be interpolated. y(t) is assumed to be a linear combination of $\{y(s^{(i)}), i=1,2,3,4\}$ weighted by normalized inversed Euclidean distances between t and $s^{(i)}$.

$$d_i = 1/||t-s^{(i)}|| \qquad i=1,2,3,4$$

$$y(t) = \left[1/\sum_{i=1}^{4} d_i\right]\left[\sum_{i=1}^{4} d_i y(s^{(i)})\right] \tag{2}$$

The justification for using the above interpolation scheme is as follows. It is a well known fact that each pixel of a rotated image is formed by contribution of its four nearest neighbors in the original image. We claim that the interpolation rule of (2) is a reasonable form of such a contribution for textures. The validity of this claim is verified by generating a 30° rotated wood grain texture from an unrotated original image by using interpolation scheme of (2). The original and the interpolated rotated textures are shown in Fig. 2. Their visual closeness implies the validity of the proposed interpolation rule.

The interpolated pixels of N_{1c} could be expanded in terms of their four neighbor grid points. Then model of Eqn. (1) could be rewritten as,

$$y(s) = \alpha \sum_{r\in N_{2c}} g_r y(s\oplus r) + \sqrt{\beta}\omega(s), \qquad s\in\Omega \tag{3}$$

where N_{2c} is a set containing (0,0) plus its 8 surronding grid corners, N_{2c} = {(-1,-1), (-1,0), (-1,1), (0,-1), (0,0), (0,1), (1,-1), (1,0), (1,1)}. The g_r coefficients are presented in Table 1.

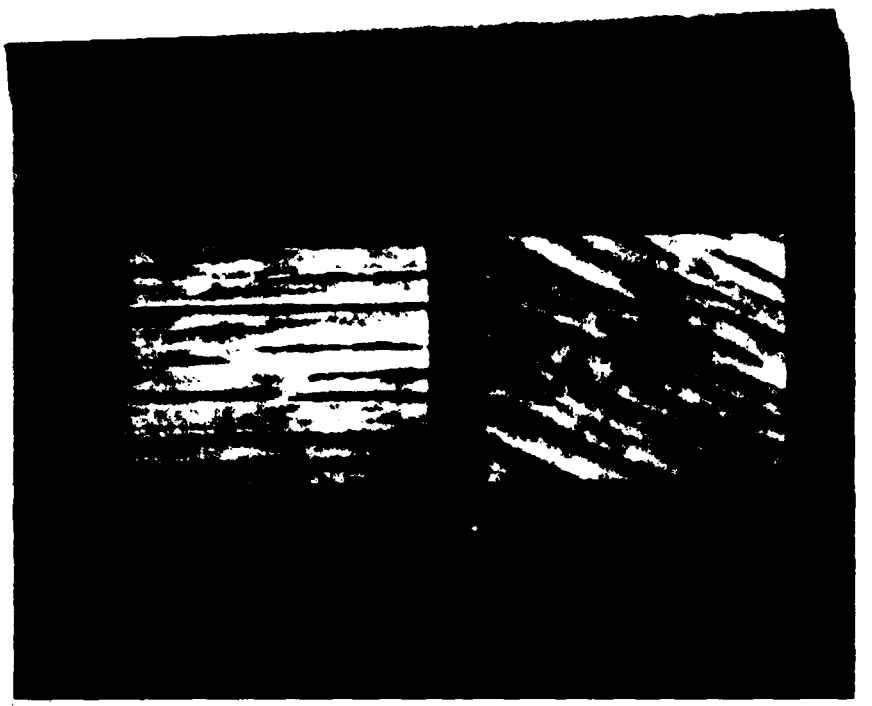

Figure 2: left : Original wood grain texture
right: Interpolated 30° rotated wood grain texture

Table 1 : Coefficients of N_{2c} set.

neighbor r	g_r
(-1,-1)	.4005
(-1,0)	1.4336
(-1,1)	.4005
(0,-1)	1.4336
(0,0)	.6636
(0,1)	1.4336
(1,-1)	.4005
(1,0)	1.4336
(1,1)	.4005

3. Parameter Estimation Algorithm

There are two popular estimation methods namely, least squares (L.S.) and maximum likelihood (M.L.) techniques. L.S. method is used to estimate the parameters of a CAR model fitted to a general natural texture. The use of M.L. estimate is ruled out because of the following reason. A general natural texture is normally nonisotropic and does not obey the ideal circular symmetry property assumed for the CAR model. It can be basically divided into two parts.

$$\mathbf{y} = \mathbf{y}_1 + \mathbf{y}_2 \tag{4}$$

where $\mathbf{y}$ represents the natural texture, $\mathbf{y}_1$ is the part of it which is rotation invariant (circularly symmetric), and $\mathbf{y}_2$ is the rotation variant (not circularly symmetric) part. When a CAR model is fitted to such a texture, it tends to only model $\mathbf{y}_1$, the rotation invariant part. $\mathbf{y}_2$ would then be part of the residuals of the model. Therefore, these residuals would be highly correlated and i.i.d. assumption is no longer valid for them. This assertion will be confirmed through an experiment in the next section. From this point on, the correlated sequence v(s) will be used in place of i.i.d. ω(s) to represent the residuals for a natural texture. Then the CAR model will change to,

$$y(s) = \alpha \sum_{r \in N_R} g_r \, y(s \oplus r) + \sqrt{\beta}\, v(s). \tag{5}$$

Since v(s) represents the rotation variant part, its correlation structure and other second order properties is of no interest to us. Our main interest lies in the rotation invariant information supplied through α and β parameters respectively. The use of the M.L. estimate is ruled out due to unavailability of such second order statistics of the image. It is also impossilble to talk about

theoretical asymptotic properties of ($\hat{\alpha}_i$, $\hat{\beta}_i$) such as their consistency or efficiency. Recall that CAR model was introduced for classification purposes. It was not intended to use it in any other application such as synthesis or restoration of images. Therefore if ($\hat{\alpha}_i$, $\hat{\beta}_i$) work well in empirical classification experiments, then there is no need to go after finding the complex correlation structure and probability density of v(s). Two slightly different L.S. estimates are presented here.

3-1. First L.S. Estimates

Let $\hat{\alpha}_1$ and $\hat{\beta}_1$ be the first L.S. estimates of α and β.

$$\text{Let} \qquad f(s) = \sum_{r \in N_{2c}} g_r y(s \oplus r). \tag{6}$$

Note that (0,0) is included in N_{2c} set. By substituting (6) into (5), the model is written as,

$$y(s) = \alpha f(s) + \sqrt{\beta} v(s), \qquad s \in \Omega. \tag{7}$$

Then L.S. estimate of α will be

$$\hat{\alpha} = \min_{\alpha} E\,[\, y(s) - \alpha\, f(s)\,]^2 \tag{8}$$

Minimizing (8) with respect to α results in,

$$\hat{\alpha}_1 = \sum_{s \in \Omega} y(s) f(s) / \sum_{s \in \Omega} f^2(s) \tag{9}$$

$$\hat{\beta}_1 = \frac{1}{M^2} \sum_{s \in \Omega} [\, y(s) - \hat{\alpha}\, f(s)\,]^2. \tag{10}$$

To calculate $\hat{\alpha}$ and $\hat{\beta}$ we need to find f(s) for each of the M^2 pixels of the image. This process could be easily described by thinking of neighbor set N_{2c}

as a mask and g_r values as the corresponding weighting factors of the components of this mask. When placed on pixel (s), this mask would only cover 8 surrounding grid points of (s) out of the whole image plus pixel (s) itself. The intensity values of the nine pixels picked by the mask are multiplied by corresponding g_r values and the results are added up to obtain f(s). By doing so, $\hat{\alpha}$ and $\hat{\beta}$ could be recursively computed. We simply move the mask pixel by pixel through the whole image and update $\sum y(s)f(s)$ and $\sum f^2(s)$ values for each pixel. Therefore, this estimation algorithm is rather fast and cheap from the memory space point of view.

3-2. Second L.S. Estimates

Another L.S. estimate for α and β could be reached by rearranging the model in the following form. Take a subset of N_{2c} as N_{3c} by excluding (0,0) element. Let $\hat{\alpha}_2$ and $\hat{\beta}_2$ denote the second L.S. estimates. Take,

$$h(s) = \sum_{r \in N_{3c}} g_r \, y(s \oplus r), \qquad N_{3c} = N_{2c} - (0,0) \tag{11}$$

By substituting (11) in (5) and using $g_{(0,0)}=.6636$, the model could be written as

$$y(s) = (\alpha_2 / 1 - .6636\ \alpha_2)\ h(s) + (\sqrt{\beta_2} / 1 - .6636\ \alpha_2)\ v(s), \qquad s \in \Omega \tag{12}$$

Take,

$$x = \alpha_2 / 1 - .6636\ \alpha_2 \tag{13}$$

$$\sqrt{y} = \sqrt{\beta_2} / 1 - .6636\ \alpha_2 \tag{14}$$

Then,

$$y(s) = x\ h(s) + \sqrt{y}\ v(s) \tag{15}$$

Take $\hat{x}$ and $\hat{y}$ as L.S. estimates of x and y.

$$\hat{x} = \min_x E\ [\ y(s) - x\ h(s)\ ]^2 \tag{16}$$

$$\hat{x} = \sum_{s\in\Omega} y(s)\ h(s)\ /\ \sum_{s\in\Omega} h^2(s). \tag{17}$$

$$\hat{y} = \frac{1}{M^2} \sum_{s\in\Omega} [\ y(s) - \hat{x}\ h(s)\ ]^2. \tag{18}$$

After finding $\hat{x}$ and $\hat{y}$, they are substituted in (13) and (14) to get $\hat{\alpha}_2$ and $\hat{\beta}_2$.

$$\hat{\alpha}_2 = \hat{x}\ (\ 1 + .6636\ \hat{x}\ ) \tag{19}$$

$$\hat{\beta}_2 = \hat{y}\ (\ 1 - .6636\ \hat{\alpha}_2\ )^2 \tag{20}$$

Calculation of $\hat{\alpha}_2$ and $\hat{\beta}_2$ is equally as easy and cheap. The only difference with the previous case is that the mask does not cover pixel (s) itself and only picks up its 8 surronding neighbors.

4. Structure of Residuals

Once $\hat{\alpha}$ and $\hat{\beta}$ are available, one can concentrate on the structure of v(s) by studying the residuals. The residuals v(s) are found by,

$$v(s) = \frac{1}{\sqrt{\beta}}\ [\ y(s) - \alpha f(s)\ ] \qquad s\in\Omega \tag{21}$$

Substituting ($\hat{\alpha}_i$, $\hat{\beta}_i$), i=1 or 2, for (α , β) in (21) gives us an estimate of v(s) sequence. This procedure was performed for a 64×64 sample of coffee beans texture. The residuals were then calculated and displayed as an image. The gray level values for both of the residual images and the original image is

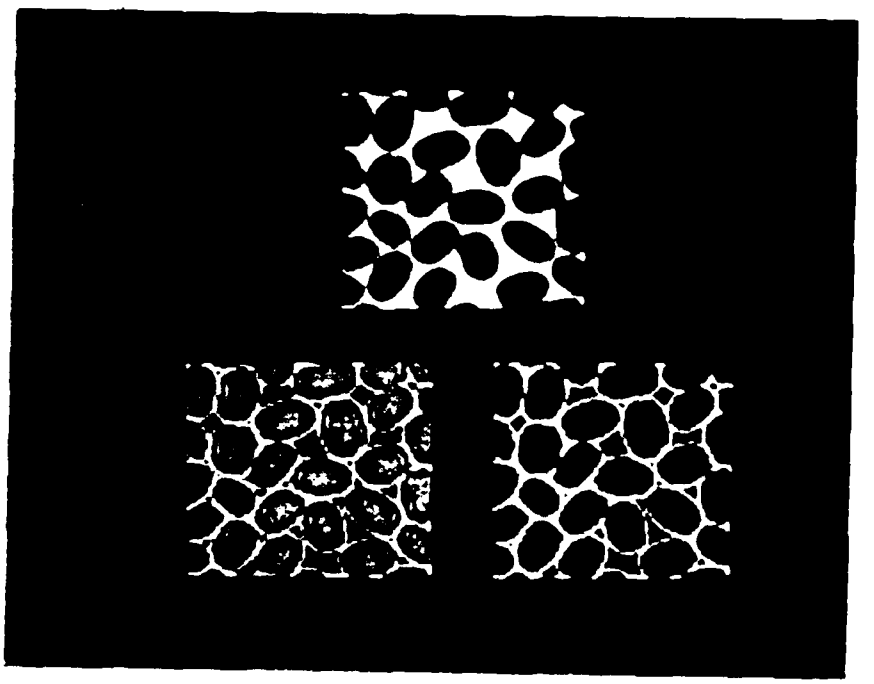

Fig. 3 : above : Original coffee beans texture

left : residuals with $\hat{\alpha}_1 = .1396$, $\hat{\beta}_1 = .0773$

right : residuls with $\hat{\alpha}_2 = .1384$, $\hat{\beta}_2 = .0774$

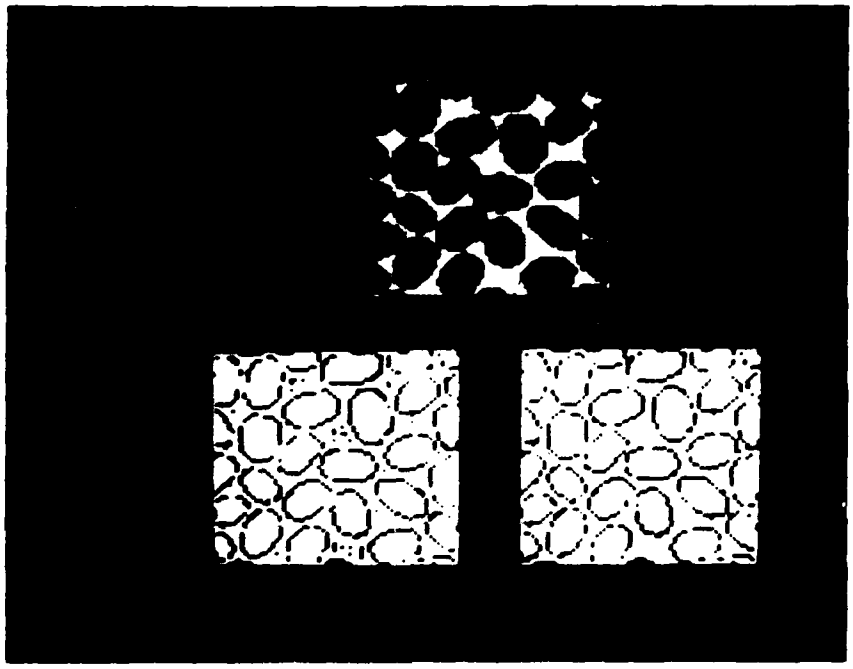

Fig. 4 : Theresholded binary images of Fig. 3

between 0 to 127. These images are shown in Fig. 3.

Some properties about v(s) sequence could be inferred by studying the residuals and comparing them with the original image. The first point to notice is the visual closeness of the two residual images with the original coffee beans texture. This proves our earlier assertion that v(s) sequence is highly correlated and i.i.d. assumption is not valid for it.

Another point to note about the residuals is that although they resemble the original image, they carry edge information which is not present in the original image. To show this property, the gray levels of images of Fig. 4 were theresholded to yield a binary image. The thereshold values were set by trial and error for the best possible result. The theresholded binary images are shown in Fig. 4. The binary residuals clearly carry edge information while the binary original image does not.

5. Rotation Invariant Features

In any classification problem a set of features need to be extracted from the image in order to reduce the dimension of data to a computationally reasonable size. Since an orientation invariant scheme is desired, the extracted features should also be orientation insensitive. One such feature set is the parameter vector of a CAR model fitted to a textured image. We claim that this vector, $(\hat{\alpha},\hat{\beta})$, obtained by either methods, is rotation invariant and show the validity of our claim through an experimental study. It should be reminded that $\hat{\beta}$ is a measure of nonisotropy or roughness of texture.

Other features could also be extracted from another class of random field models known as Simultaneous Auto Regressive (SAR) models. The details of this class of models and the iterative method for the Maximum Likelihood

estimation of their parameters could be found in [15] and [4]. Briefly stated, a SAR model has the following form,

$$y(s) = \sum_{r \in N} \theta_r y(s \oplus r) + \sqrt{\rho}\omega(s), \qquad s \in \Omega \tag{22}$$

where the neighbor set N is an appropriate subset of integer pairs with (0,0) excluded. N obeys the same labelling convention used before.

M.L. estimate of ρ is denoted by ρ^*. ρ^* of a simultaneous auto regressive model fitted to an image is a relative measure of fineness of the texture of that image regardless of the neighbor set N used. Fineness is a property that does not change under rotation. Therefore, ρ^* of a SAR model with a symmetric neighbor set $N_1 = \{(1,0), (-1,0), (0,1), (0,-1)\}$ could be a useful rotation invariant feature.

Another extractable feature from SAR models is a measure of directionality in the texture. M.L. estimates, θ_r^*, of SAR models show the amount of dependency of an image pixel to one of its neighboring pixels (r). The extent of variation of such a dependency in orthogonal directions is one such measure. Orthogonal directions in the image plane consists of two directional pairs, namely (horizontal, vertical), and (diagonal, off-diagonal). These pairs could be represented by neighbor sets N_1 and N_2 where, $N_1 = \{(1,0), (-1,0), (0,1), (0,-1)\}$, and $N_2 = \{(1,1), (-1,-1), (1,-1), (-1,1)\}$. A SAR model with neighbor set N_1 is fitted to the texture and the M.L. estimates of its parameters, $(\theta^*_{(1,0)}, \theta^*_{(0,1)})$ is calculated. Then a different SAR model with neighbor set N_2 is used to find $(\theta^*_{(1,1)}, \theta^*_{(1,-1)})$. A function of these four parameters ς, where $\varsigma = \text{Max}(| \theta^*_{(1,0)} - \theta^*_{(0,1)} | , | \theta^*_{(1,1)} - \theta^*_{(1,-1)} |)$ corresponds to extent of variation in orthogonal directions could also be extracted as a rotation invariant feature. The rotation independency of ρ^* and ς are

investigated in the next section. More discussions about these four proposed features and their class separability power is provided in the experimental study section.

6. Experimental Study

Let $\{y''(s), s\in\Omega\}$ be the set of grid point intensities of a M×M digitized image. It is a well known fact that the first order statistics of $\{y''(s)\}$ can be directly affected by changes in illumination or quantizing schemes. To overcome such effects all the images are subjected to a gray scale normalization procedure described in [12]. This algorithm flattens the images histograms and guarantees that all the samples have identical first-order gray level statistics. Let $\{y'(s), s\in\Omega\}$ be the histogram flattened version of $\{y''(s)\}$. The images are also normalized to have zero empirical mean and unit empirical variance. If $\{y(s), s\in\Omega\}$ denote the normalized image then,

$$y(s) = (y'(s)-a) / \sigma, \tag{23}$$

$$\text{where,} \quad a = \frac{1}{M^2} \sum_{s\in\Omega} y'(s), \tag{24}$$

$$\sigma^2 = \frac{1}{(M^2-1)} \sum_{s\in\Omega} (y'(s)-a)^2. \tag{25}$$

Note that a and σ^2 will be the same for all the samples. Throughout the experimental study we always use the normalized zero mean unit variance version of an input textured image.

Twelve different textures, (a) Calf leather (D24), (b) wool (D19), (c) beach sand (D29), (d) pig skin (D92), (e) plastic bubbles (D112), (f) herringbone weave (D17), (g) raffia (D84), (h) wood grain (D68), (i) grass (D9), (j) straw (D15), (k)

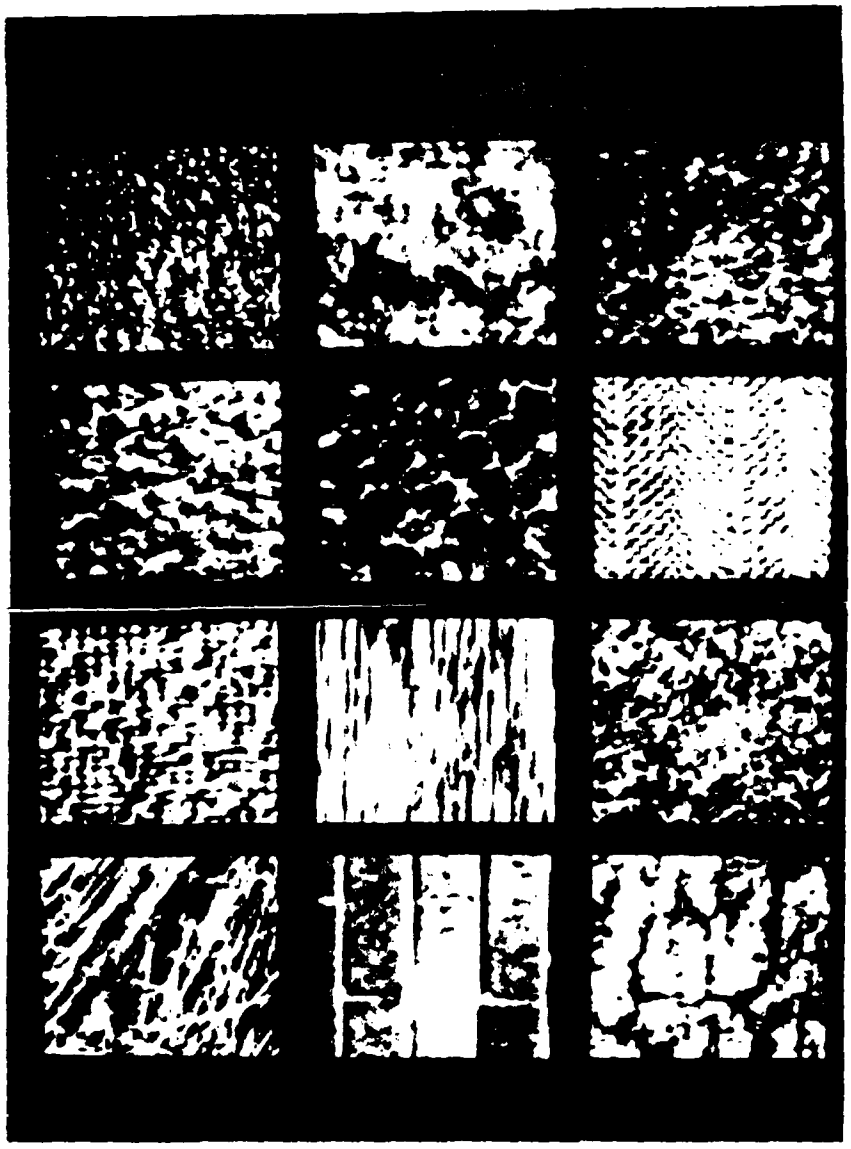

Fig 5 : 0°, 64×64 windows of textures.

From above left to right :

calf leather, wool, sand, pig skin, plastic bubbles, heringbone weave, raffia, wood, grass, straw, brick wall, bark of tree.

brick wall (D95), (l) bark of tree (D12) were chosen from the photo album by Brodatz [2]. Seven rotated 512×512 digitized images with relative angles of rotation of 0°, 30°, 60°, 90°, 120°, 150°,, and 200° are taken from each class of texture. The gray scale value range is between 0 and 255. Each 512×512 image was first reduced to a 128×128 by averaging every 4×4 window into a single pixel. Each 128×128 image is then segmented into 4 64×64 images. 2 of them are used for training and the remaining 2 for testing. Therefore 14 training and 14 test samples from each class of textures are available. One of the 64×64 digitized window of 0° rotated version of each texture is shown in Fig.5

To get the features the CAR model is fitted to each of the training images and its parameter vector $(\hat{\alpha},\hat{\beta})$ is estimated by one of the discussed methods. Two different SAR models with neighbor sets N_1 and N_2 are also used to extract ρ^* and ς respectively from all the training images.

6-1. Properties of the Features

Before proceeding with classification experiments, we should confirm the validity of the rotation invariancy of the suggested feature vector. To do so the sample means and standard deviations of differently oriented samples of each texture is calculated. Tables 2 and 3 summarize the results for raffia texture. There are 4 unidirectional samples per rotation per texture. The sample means and standard deviations of all the four features for each of the respective rotations are presented. The numbers in Table 2 show that $\hat{\alpha}_1$ values for different orientations are very close to each other. The smallness of their standard deviations is an indication that very little variation exists among the 4 $\hat{\alpha}_1$ values of each rotation. The same argument holds for $\hat{\beta}_1$ values

although the standard deviations are generally bigger than those of $\hat{\alpha}_1$. Therefore both $\hat{\alpha}_1$ and $\hat{\beta}_1$ could be taken as good rotation invariant features. The ρ^* and ς values are not as tightly close as $\hat{\alpha}_1$ and $\hat{\beta}_1$ although they are close enough to be taken as rotation invariant.

Table 3 exhibits the results for $\hat{\alpha}_2$ and $\hat{\beta}_2$. The ρ^* and ς values are the same ones as Table 2. The same arguments could be repeated here. Again $\hat{\alpha}_2$ and $\hat{\beta}_2$ values are tightly closed and rotation invarint. Notice that $\hat{\alpha}_2$ are generally smaller than $\hat{\alpha}_1$ and $\hat{\beta}_2$ is very close to $\hat{\beta}_1$. The values for other eleven textures which are not presented here due to space considerations also support the validity of our ascertation.

The overall sample means and standard deviations of all the 14 training features for each texture are also tabulated in Tables 4 and 5. Note that these numbers include the overall effect of all the seven rotations. Studying the values of Table 3 reveals that $\hat{\alpha}_1$ values for differemt classes are very close together except for herringbone weave and raffia textures. It should also be mentioned that the standard deviation of $\hat{\alpha}_1$ is very small for all the classes. This suggests that these values do not change much and although they are close, but they contain some class separability property. On the other hand $\hat{\beta}_1$ values show more class separability property and are not so close to each other. Note that $\hat{\beta}_1$ is large for herringbone weave which is highly circularly non-symmetric and and is small for plastic bubbles which is not. The standard deviations of them are also small. The fineness feature ρ^* is high for busy textures such as calf leather, grass, sand , and weave. The standard deviation of ρ^* are generally higher than $\hat{\beta}_1$. This property can be seen very clearly for wood and straw textures. Since both ρ^* and $\hat{\beta}_1$ measure the roughness of texture to some degree, then they may carry similar information. Their values

Table 2 : Sample means and standard deviations of features of raffia texture.
(4 unidirectional 64×64 samples per angle)

Features

	$\hat{\alpha}_1$		$\hat{\beta}_1$		ρ^*		ς	
Rotation Angle	Mean	STD	Mean	STD	Mean	STD	Mean	STD
0°	.1750	.0050	.3465	.0106	.3599	.0086	.0965	.0144
30°	.1717	.0039	.3804	.0038	.4920	.0070	.0521	.0313
60°	.1701	.0045	.3705	.0098	.4461	.0125	.0963	.0192
90°	.1737	.0057	.3388	.0206	.3517	.0203	.1040	.0102
120°	.1693	.0027	.3753	.0145	.4801	.0223	.0586	.0277
150°	.1701	.0070	.3723	.0154	.4508	.0215	.1001	.0089
200°	.1709	.0073	.3601	.0106	.4276	.0140	.0634	.0313

Table 3 : Sample means and standard deviations of features of raffia texture. (4 unidirectional 64×64 samples per angle)

	Features							
	$\hat{\alpha}_2$		$\hat{\beta}_2$		ρ^*		ς	
Rotation Angle	Mean	STD	Mean	STD	Mean	STD	Mean	STD
0°	.1628	.0041	.3496	.0109	.3599	.0086	.0965	.0144
30°	.1581	.0033	.3843	.0039	.4920	.0070	.0521	.0313
60°	.1573	.0037	.3741	.0100	.4461	.0125	.0963	.0192
90°	.1620	.0044	.3417	.0212	.3517	.0203	.1040	.0102
120°	.1564	.0025	.3789	.0149	.4801	.0223	.0586	.0277
150°	.1572	.0058	.3759	.0159	.4508	.0215	.1001	.0089
200°	.1586	.0060	.3634	.0110	.4276	.0140	.0634	.0313

Table 4 : Sample means and standard deviations of training features utilized in classification.
(14 differently oriented 64×64 samples per class)

	Features							
	$\hat{\alpha}_1$		$\hat{\beta}_1$		ρ^*		ς	
TEXTURE	Mean	STD	Mean	STD	Mean	STD	Mean	STD
Calf Leather	.1553	.0049	.5595	.0420	.6401	.0705	.2000	.0256
Wool	.1447	.0023	.2149	.0124	.2444	.0175	.0521	.0143
Sand	.1563	.0023	.4076	.0166	.4903	.0266	.0586	.0201
Pig skin	.1553	.0016	.3211	.0145	.3818	.0196	.0626	.0223
Pl. Bubbles	.1445	.0016	.2069	.0104	.2312	.0170	.0453	.0162
Herringbone	.1763	.0099	.6951	.0311	.8342	.0290	.0251	.0097
Raffia	.1718	.0055	.3656	.0208	.4328	.0566	.0802	.0297
Wood	.1474	.0054	.3530	.0395	.2030	.1190	.4984	.0263
Grass	.1475	.0034	.4710	.0179	.5710	.0226	.0753	.0135
Straw	.1407	.0057	.3675	.0696	.3171	.1740	.3743	.0771
Brick	.1451	.0027	.2258	.0308	.2349	.0589	.2511	.0539
Tree	.1454	.0008	.2236	.0200	.2521	.0287	.0908	.0217

Table 5 : Sample means and standard deviations of training features utilized in classification.
(14 differently oriented 64×64 samples per class)

	Features							
	$\hat{\alpha}_2$		$\hat{\beta}_2$		ρ^*		ς	
TEXTURE	Mean	STD	Mean	STD	Mean	STD	Mean	STD
Calf Leather	.1325	.0071	.5690	.0437	.6401	.0705	.2000	.0256
Wool	.1405	.0019	.2156	.0125	.2444	.0175	.0521	.0143
Sand	.1438	.0014	.4114	.0171	.4903	.0266	.0586	.0201
Pig skin	.1469	.0016	.3232	.0147	.3818	.0196	.0626	.0223
Pl. Bubbles	.1406	.0013	.2053	.0129	.2312	.0170	.0453	.0162
Herringbone	.1228	.0111	.7230	.0335	.8342	.0290	.0251	.0097
Raffia	.1590	.0048	.3691	.0213	.4328	.0566	.0802	.0297
Wood	.1386	.0054	.3553	.0401	.2030	.1190	.4984	.0263
Grass	.1332	.0023	.4760	.0185	.5710	.0226	.0753	.0135
Straw	.1319	.0045	.3700	.0709	.3171	.1740	.3743	.0771
Brick	.1406	.0022	.2266	.0311	.2349	.0589	.2511	.0539
Tree	.1409	.0008	.2243	.0202	.2521	.0287	.0908	.0217

have the same trend for all the textures. When $\hat{\beta}_1$ is high so is ρ^* and vice versa. This suggests that only one of them may be useful as a feature for classification. Since $\hat{\beta}_1$ is a better and more consistent rotation invariant value with smaller standard deviations, then it would be preferred over ρ^*. The extent of variations in orthogonal directions, ς, is only high for wood grain, calf leather, straw, and brick and is tightly close for the other textures. Again some class separability power could be detected in this feature making it useful in recognition of the texture.

The same arguments also hold for ($\hat{\alpha}_2,\hat{\beta}_2,\rho^*,\varsigma$) values given in Table 5. Notice that $\hat{\alpha}_2$ values are generally smaller than their $\hat{\alpha}_1$ counterparts. Since both $(\hat{\alpha}_1,\hat{\beta}_1)$ and $(\hat{\alpha}_2,\hat{\beta}_2)$ basically follow the same trend, it will be logical to expect that they be equally useful as classifying features. A set of classification experiments were performed in order to evaluate these features and the disscussed observations about them.

6-2. Classification Experiments

As the first experiment, classification of the test samples using $(\hat{\alpha}_1,\hat{\beta}_1,\rho^*,\varsigma)$ as the feature vector is tried. The classifier used in this study is a distance classifier which basically measures a weighted distance of the feature set of the test sample to the mean of the training samples of each class. The test sample is then classified to the class which exhibits the lowest distance. Details of this classifier is presented in [16]. The classification result is tabulated in Table 6 in the form of a confusion matrix. To the left of the matrix, the textures are listed. Each row shows how a specific set of samples was classified. The diagonal numbers show how many out of 14 test samples for each class were correctly classified. for example all 14 test samples of leather were classified

correctly while only 9 wool samples were recognized as wool. 3 of them were incorrectly classified as plastic bubbles and 2 as bark of tree. A total classification rate of 92% is achieved. Classification rates for individual classes are listed to the right of each row. 8 of the classes are classified with 100 percent accuracy. The classification results of the other 4 classes are 93, 79, 64, and 64 percent. This result shows that there is a strong classification power in $(\hat{\alpha}_1,\hat{\beta}_1,\rho^*,\varsigma)$.

The same experiment performed in the previous case was repeated with ($\hat{\alpha}_2,\hat{\beta}_2,\rho^*,\varsigma$). Table 7 is the result of classification experiment with the same 12 textures. A classification rate of 92% is achieved. The results are the same as the previous case. This the previous observation that both L.S. estimates of CAR parameters , although different, basically carry the same classification power. In order to investigate the classification power of smaller number of features, two more experiments were performed. In the first experiment ($\hat{\alpha}_2$, $\hat{\beta}_2$) were used as the features and the other two features were dropped. The result is presented in Table 8. An overall classification rate of 69% is an indication of some classification power but apparently not enough. In the second experiment ($\hat{\alpha}_2$, $\hat{\beta}_2$, ς) were utilized. Table 9 shows the outcome of the experiment. 91% accuracy rate is an indication that the dropped feature set ρ^* carries little classification power and we could do almost as good without using it, although its utilization will increase the accuracy rate by one percent. This supports our other suggestion that both $\hat{\beta}_2$ and ρ^* carry the same information. In the third experiment (ρ^*,ς) is used and the CAR parameters are dropped. Table 10 shows the result. Again a 79% classification rate is an indication of a not very powerful feature set.

	Assigned Class												Class.
	L.	W.	S.	P.	B.	H.	R.	W.	G.	S.	B.	T.	acc. %
Calf Leather	14												100
Wool		9			3							2	64
Beach Sand			14										100
Pig Skin				14									100
Plastic Bubbles		2			11							1	79
Herringbone						14							100
Raffia				1			13						93
Wood Grain								14					100
Grass									14				100
Straw	1							4		9			64
Brick											14		100
Tree												14	100

Table 6 : Classification result using $(\hat{\alpha}_1 , \hat{\beta}_1 , \rho^* , \varsigma)$ as feature.
Total error: 14 in 168 test samples.
Classification rate: 92%.

	Assigned Class												Class.
	L.	W.	S.	P.	B.	H.	R.	W.	G.	S.	B.	T.	acc. %
Calf Leather	14												100
Wool		9			3							2	64
Beach Sand			14										100
Pig Skin				14									100
Plastic Bubbles		2			11							1	79
Herringbone						14							100
Raffia				1			13						93
Wood Grain								14					100
Grass									14				100
Straw	1							4		9			64
Brick											14		100
Tree												14	100

Table 7 : Classification result using $(\hat{\alpha}_2 , \hat{\beta}_2 , \rho^* , \varsigma)$ as feature.
Total error: 14 in 168 test samples.
Classification rate: 92%.

	Assigned Class												Class.
	L.	W.	S.	P.	B.	H.	R.	W.	G.	S.	B.	T.	acc. %
Calf Leather	13											1	93
Wool		2			6						3	3	14
Beach Sand			12					2					86
Pig Skin				14									100
Plastic Bubbles		1			12							1	86
Herringbone						14							100
Raffia				1			13						93
Wood Grain				3				6	1	4			43
Grass									14				100
Straw								3	3	8			57
Brick				1	5						6	2	43
Tree		1			4						7	2	14

Table 8 : Classification result using $(\hat{\alpha}_2 , \hat{\beta}_2)$ as feature.
Total error: 52 in 168 test samples.
Classification rate: 69%.

	Assigned Class												Class.
	L.	W.	S.	P.	B.	H.	R.	W.	G.	S.	B.	T.	acc. %
Calf Leather	14												100
Wool		8			4							2	57
Beach Sand			14										100
Pig Skin				14									100
Plastic Bubbles		3			10							1	71
Herringbone						14							100
Raffia				1			13						93
Wood Grain								14					100
Grass									14				100
Straw	1							4		9			64
Brick											14		100
Tree												14	100

Table 9 : Classification result using $(\hat{\alpha}_2 , \hat{\beta}_2 , \varsigma)$ as feature.
Total error: 16 in 168 test samples.
Classification rate: 91%.

	Assigned Class												Class.
	L.	W.	S.	P.	B.	H.	R.	W.	G.	S.	B.	T.	acc. %
Calf Leather	14												100
Wool		6			4							4	43
Beach Sand			11				2		1				79
Pig Skin				13					1				93
Plastic Bubbles		5			8							1	57
Herringbone						14							100
Raffia			4	4			6						43
Wood Grain								14					100
Grass									14				100
Straw	1							4		7	2		50
Brick										3	11		79
Tree												14	100

Table 10 : Classification result using (ρ^*, ς) as feature.
Total error: 36 in 168 test samples.
Classification rate: 79%.

6-3. Experiments with Less Condensed Textures

In order to show the robustness of the proposed feature set, another set of experiments were performed with some of the previous textures viewed from a closer distance. This was achieved by reducing each 512×512 image to a 256×256 instead of a 128×128 by averaging each 2×2 window into one pixel. The 256×256 image was then segmented into 16 64×64 windows, 8 of which used for training and the remaining 8 for testing. Since 7 rotated images exists for each class of textures, then 56 training and 56 test samples are available for each class. One of the 64×64 digitized window of 0° rotated version of each texture is shown in Fig. 6. Comparison of these textures with those presented in Fig. 5 can convey the scale difference property. Three classes of textures namely, brick wall, straw, and bark of tree were dropped from the database. The reason was since each 64×64 window contains more dispersed texture, then we tend to lose the basic texture in these classes. For example the micotexture inside each brick will be more dominant in a 64×64 window than the structure of the brick wall itself.

The classification results with ($\hat{\alpha}_1$, $\hat{\beta}_1$, ς) and ($\hat{\alpha}_2$, $\hat{\beta}_2$, ς) are presented in Tables 11 and 12. Note that ρ^* is not used because the experiments showed that it will not improve the results. Classification accuracies of 96% and 97% indicates that the proposed method works for this database as well and its performance is not limited to one particular set.

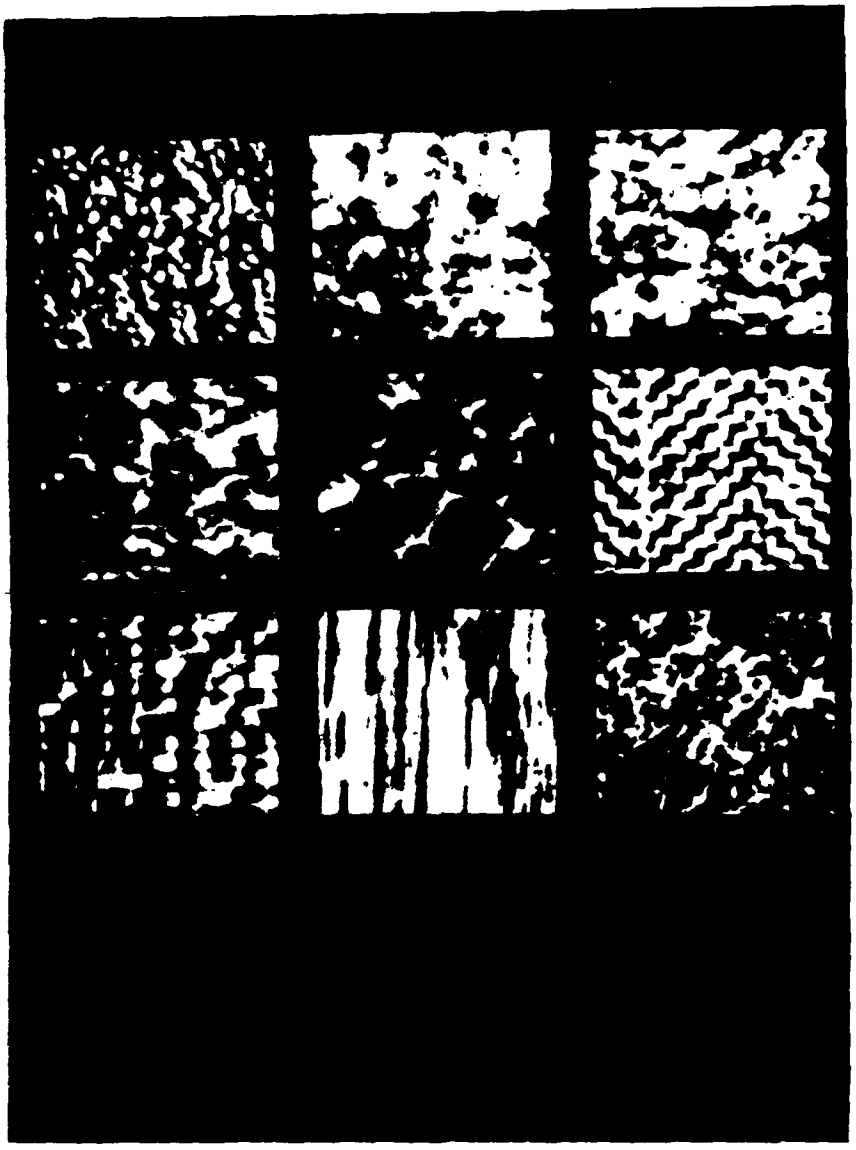

Fig 6 : 0 °, 64×64 windows of less condensed textures.

From above left to right :

calf leather, wool, sand, pig skin, plastic bubbles, heringbone weave, raffia, wood, grass.

	Assigned Class									Class.
	L.	W.	S.	P.	B.	H.	R.	W.	G.	acc. %
Calf Leather	55								1	98
Wool		53		2	1					95
Beach Sand			53	2			1			95
Pig Skin			6	50						90
Plastic Bubbles		1		2	53					95
Herringbone						56				100
Raffia			2				54			93
Wood Grain								56		100
Grass									56	100

Table 11 : Classification result using $(\hat{\alpha}_1 , \hat{\beta}_1 , \varsigma)$ as feature.
Total error: 18 in 504 test samples.
Classification rate: 96%.

	Assigned Class									Class.
	L.	W.	S.	P.	B.	H.	R.	W.	G.	acc. %
Calf Leather	55								1	98
Wool		54		1	1					96
Beach Sand			53	2			1			95
Pig Skin			4	52						93
Plastic Bubbles			3		53					95
Herringbone						56				100
Raffia			2				54			93
Wood Grain								56		100
Grass									56	100

Table 12 : Classification result using $(\hat{\alpha}_2 , \hat{\beta}_2 , \varsigma)$ as feature.
Total error: 15 in 504 test samples.
Classification rate: 97%.

7. Discussion of the Results

The experimental results showed that the two different L.S. estimates of CAR parameters, $(\hat{\alpha}_1,\hat{\beta}_1)$ and $(\hat{\alpha}_2,\hat{\beta}_2)$, basically carry the same classification power and neither one really can be preferred over the other. Furthermore the experiments confirmed that $\hat{\beta}_i$ and ρ^* contain similar information about the degree of roughness of the texture and only one of them could be useful for classification. $\hat{\beta}_i$ was preferred over ρ^* since it is a more consistent rotation invarint feature with smaller standard deviation values. In fact dropping ρ^* from the feature set resulted in only one percent or less decline in overall classification rate. $\hat{\beta}_i$ and ς features exhibit a more pronounced class separibility property than $\hat{\alpha}_i$. Experiments with reduced number of features suggested that although their combined effect is very powerful, each of them individually is not very powerful. 92 percent accuracy rate obtained with 12 different classes of natural textures is an indication of the power and appropriateness of the feature set.

Experiments with a different resolution database showed the generality and robustness of the method. A 97 percent accuracy rate obtained with 9 higher resolution classes of textures is a very good result.

The method was implemented on a PDP-11/45 computer. Feature extraction from each 64×64 digitized texture takes around two minutes. Its classification only takes a fraction of seconds. Therefore the method is fast and as mentioned before requires very little memory space.

It should be noted that although the experiments were carried out using seven rotation angles, the method is generally orientation independent and works for any arbitrary oriented train and test samples of texture.

8. Summary and Conclusions

An algorithm for extracting a couple of rotation invariant features based on a new class of random field models, called circular auto regressive (CAR) models, was developed. The estimated parameters of this model when fitted to a texture are taken as the desired features.

A different class of random field models known as simultaneous auto regressive (SAR) models was utilized in order to obtain two more rotation invariant features. One being a measure of the fineness of the texture, and the other a measure of the extent of variations of the texture in orthogonal directions.

The classification power of these features was investigated in classification experiments involving twelve and nine different natural textures with samples having different orientation. It was concluded that the combined effect of these features carries a strong classification power for a database consisting of both microtextures and macrotextures. Considering that this study was done in spatial domain and only four features were used, a 92% and 97% classification rate for arbitrary placed texture is a rather promising and encouraging result.

References

[1] R. Bajcsy, "Computer description of textured surfaces," *Proc. 3rd Int. Joint Conf. Art. Int.*, pp. 572-579, Aug. 1973.

[2] P. Brodatz, *Texture: A Photographic Album for Artists and Designers,* Dover, New York, N.Y., 1956.

[3] L. Carlucci, "A formal system for texture languages," *Pattern Recognition,* vol. 4, pp. 53-72, 1972.

[4] R. Chellappa, and R. L. Kashyap, "Synthetic generation and estimation in random field models for images," *IEEE Computer Soc. Conf. on Pattern Recog. and Image Proc.*, pp. 577-582, Dallas, TX, Aug. 1981.

[5] D. Chetverikov, "Experiments in the rotation-invariant texture discrimination using anisotropy features," Proc. 6th Int. Conf. on Pattern Recognition, pp. 1071-1073, Munich, Germany, Oct. 1982.

[6] R. W. Conners, and C. A. Harlow, "A theoretical Comparison of texture algorithms," *IEEE Trans. on Pattern Anal. and Machine Intel.*, vol. PAMI-2, No. 3, pp. 204-222, May 1980.

[7] R. W. Conners and C. A. Harlow, "Toward a structural textural analyzer based on statistical methods," *Computer Graphics and Image Processing,* vol. 12, pp. 224-256, 1980.

[8] L. S. Davis, S. Johns, and J. K. Aggrawal, "Texture analysis using generalized co-occurrence matrices," *IEEE Trans. on Pattern Anal. and Machine Intel.*, vol. PAMI-1, pp. 251-259, July 1979.

[9] L. S. Davis, M. Clearman, and J. K. Aggrawal, "An empirical evaluation of generalized co-occurrence matrices," *IEEE Trans. on Pattern Anal. and Machine Intel.*, vol. PAMI-3, No. 2, pp. 214-221, March 1981.

[10] L. S. Davis, "Polagrams: A new tool for image texture analysis," *Pattern Recognition*, vol. 13, No. 3, pp. 219-223, 1981.

[11] M. Galloway, "Texture analysis using gray-level run lengths," *Computer Graphics and Image Processing*, vol. 4, pp. 172-199, 1974.

[12] R. C. Gonzalez, and P. Wintz, "Digital Image Processing," Addison-Wesley, Reading, MA, 1977, pp. 119-127.

[13] R. M. Haralick, K. Shanmugam, and I. Dinstein, "Textural features for image classification," *IEEE Trans. on Syst., Man, and Cybern.*, vol. SMC-3, No. 6, pp. 610-621, Nov. 1973.

[14] R. M. Haralick, "Statistical and structural approaches to texture," *Proc. of IEEE*, vol. 67, No. 5, pp. 786-804, May 1979.

[15] R. L. Kashyap, "Analysis and synthesis of image patterns by spatial interaction models," *Progress in Pattern Recognition*, Edited by L. N. Kanal, and A. Rosenfeld, vol. 1, North-Holland, New York, 1981, pp. 149-186.

[16] R. L. Kashyap, R. Chellappa, and A. Khotanzad, "Texture classification using features derived from random field models," *Pattern Recognition Letters*, vol. 1, pp. 43-50, Oct. 1982.

[17] R.L. Kashyap, and A. Khotanzad, "Rotation invariant texture classification using circular random field models," *IEEE Computer Soc. Conf. on Computer Vision and Paterrn Recog.*, Arlington, VA, June 19-23 1983.

[18] S. Y. Lu, and K. S. Fu, "A syntactic approach to texture analysis," *Computer Graphics and Image Processing*, vol. 7, pp. 303-330, 1978.

[19] F. Tomita, Y. Shirai, and S. Tsuji, "Classification of textures by a structural analysis," *Proc. of the 4th Int. Joint Conf. on Pattern Recognition*, pp. 556-558, Kyoto, Japan, Nov. 1978.

[20] A. L. Vickers and J. W. Modestino, "A maximum likelihood approach to texture classification," *IEEE Trans. on Pattern Anal. and Machine Intel.*, vol. PAMI-4, No. 1, pp. 61-68, Jan. 1982.

[21] F. M. Vilnrotter, "Structural analysis of natural textures," *Ph.D. Dissertation*, TR No. USCISG 100, USCIPI 1040, Departments of Electrical Engr. and Computer Science, University of Southern California, Los Angeles, CA, Sept. 1981.

[22] J. S. Weszka, C. R. Dyer, and A. Rosenfeld, "A comparative study of texture measures for terrain classification," *IEEE Trans. on Syst., Man, and Cybern.*, vol. SMC-6, No. 4, pp. 269-285, April 1976.

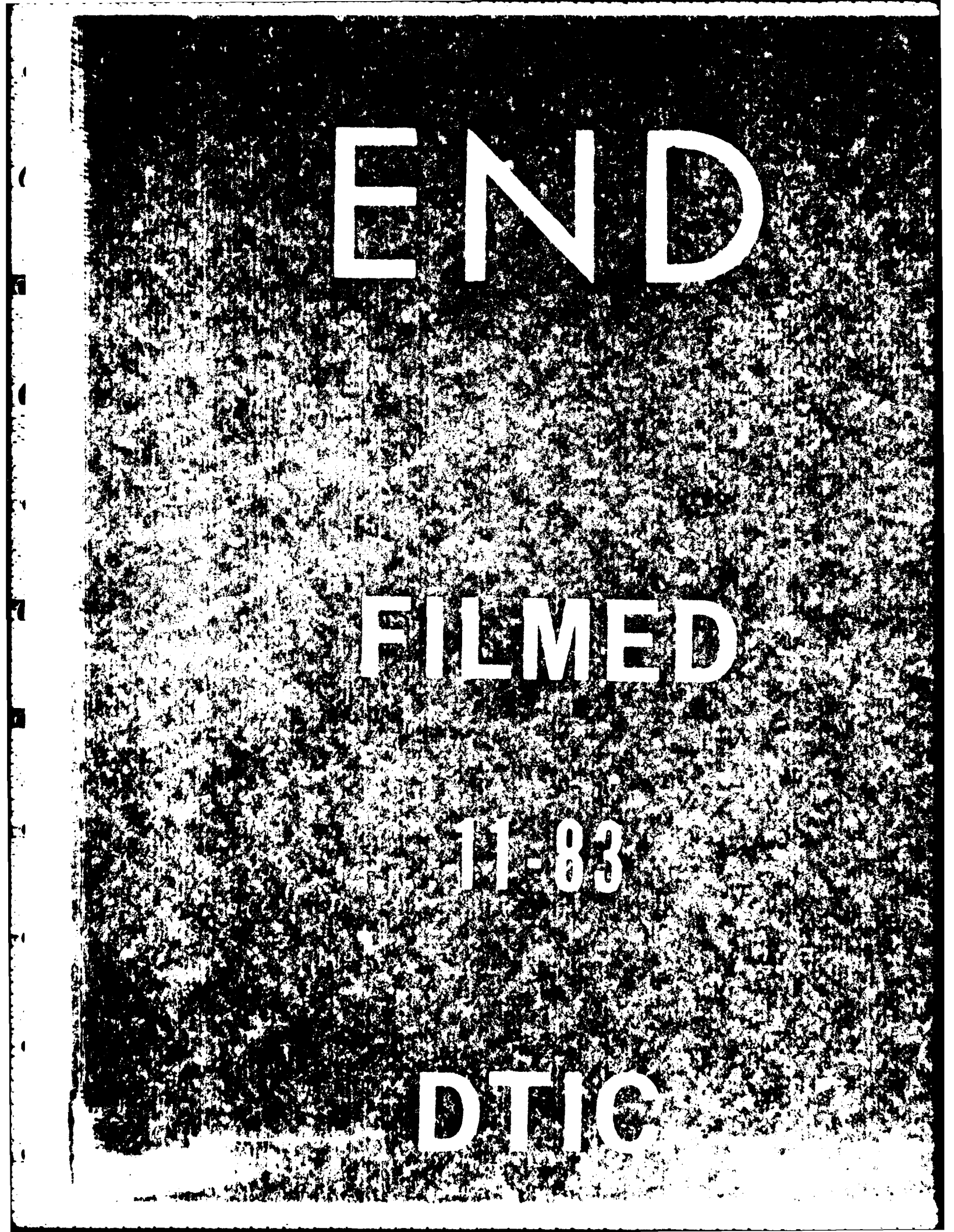
END
FILMED
11-83
DTIC